

ADSORPTION PROPERTIES OF MAGNETITE NANOPARTICLES FOR THE REMOVAL OF HEAVY METALS FROM AQUEOUS SOLUTION

Eman R. Zaki^{1,*}; Saber M. Ahmed¹; Omnia I. Ali²
and Mohga S. Abdalla²

¹Soil, Water and Environment Research Institute, Agriculture Research Centre, Giza, Egypt

²Chemistry Department, Faculty of Science, Helwan University, Cairo, Egypt

*E-mail- amanrabea1987@gmail.com

ABSTRACT

This study investigated the applicability of magnetite nanoparticles as a powerful adsorbent for the batch-mode removal of Cd(II) and Pb(II) ions from aqueous solutions. The magnetite nanoparticles, synthesized by the chemical co-precipitation technique, were characterized using XRD, SEM-EDX, TEM, and FT-IR measurements. The influence of the initial pH, contact time, mass of magnetite, and initial metal ion concentration on the removal efficiency of Cd(II) and Pb(II) ions was investigated. Adsorption data were consistent with the Langmuir isotherm and pseudo-second order kinetics. The adsorption of Cd(II) and Pb(II) ions by magnetite nanoparticles was demonstrated by the thermodynamic parameters to be an endothermic and favorable process. Utilizing HCl, magnetite adsorbent can be efficiently regenerated up to five times. It can be concluded that magnetite nanoparticles can be used as an environmentally friendly alternative adsorbent to remove Cd(II) and Pb(II) ions from aqueous solutions.

Key Words: Magnetite nanoparticles, removal of heavy metal ions, water pollution.

INTRODUCTION

Water pollution is becoming a critical worldwide concern with the progress in human life and the proliferation of industries. Wastewater effluents from industrial activities, sewage sludge, agricultural activities, and environmental changes directly affect human and soil pollution (Afolabi *et al.*, 2021). There are different kinds of contaminants such as, bacteria, viruses, pesticides, organic compounds, fertilizers, dyes, and heavy metal ions (Baby *et al.*, 2019). Among all of these water contaminants, heavy metals are the most common pollutant present in environmental waters around the world (Vardhan *et al.*, 2019). They mainly reach the environment and water through industrial activities from metallurgical, nuclear, batteries, leather, pesticides, pharmaceuticals, fertilizers, paper, petroleum and textile industries (Beni and Esmaeili, 2020). These heavy metals can be toxic even at low concentrations. They are non-biodegradable in nature and therefore bio-

accumulate in living organisms. This causes severe health problems in animals, plants, and human beings including headaches, anemia, still birth, growth retardation, malfunctioning of the nervous system, kidney failure, brain damage, metabolic acidosis, oral ulcers, and cancer (**Baby et al., 2019 ; Akpomie and Conradie, 2020**). Among heavy metals, cadmium and lead are considered the most dangerous and can cause serious health problems even at extremely low levels, including cancer, reproductive problems, and effects on embryonic development (**Zhang et al., 2021**). The Environmental Protection Agency states that the maximum amount of lead and cadmium in drinking water is 0.015 mg L^{-1} and 0.005 mg L^{-1} , respectively (**Abatal et al., 2021**). Thus, the removal of heavy metals from wastewater before being discharged has received significant attention. Decontamination of heavy metal ions from aqueous solutions has been performed by a variety of approaches, including flotation, ion exchange, sedimentation, electrochemical treatment, precipitation, filtration, coagulation, ozonation, flocculation, evaporation, and adsorption (**Akpomie and Conradie, 2020 ; Umeh et al., 2020 ; Yu and Jiang, 2020**). Among these various techniques, adsorption has been widely used due to its high efficiency, cost effectiveness, ease of application, and guarantee of complete removal at low concentrations (**Liu et al., 2020**). Many adsorbents have been used for Cd(II) and Pb(II) removal, but keen interest exists in improved and advanced low-cost adsorbents with high surface areas and adsorption capacities (**Rajput et al., 2016**). Nanoadsorbents are sought because their small particle sizes, high specific surface areas, and high porosity enhance chemical reactivity and adsorbate/adsorbent interactions, allowing them to isolate contaminants over a wide concentration range quickly and efficiently while releasing no toxic payload (**Kumari et al., 2019**). Among these nanoadsorbents, iron oxide has gained special attention in water purification to remediate heavy metals from water (**Geneti et al., 2022**), which could be attributed to their high surface area, chemical stability, easy synthesis, low toxicity, and magnetic properties (**Zhou et al., 2020**). Therefore, magnetic separation and adsorption have been combined to remove heavy metal ions from contaminated water in order to enhance the decontamination process. Magnetite nanoparticles can be synthesized using a variety of techniques, including hydrothermal synthesis, thermal decomposition, co-precipitation, sol-gel method, and colloidal chemistry method. Co-precipitation has emerged as the most promising method for the synthesis of nanomaterials as the procedure is relatively simple and the particles may be produced with a regulated particle size.

Here in, magnetite nanoparticles were synthesized using the co-precipitation method. The magnetite nanoparticle's surface and chemical properties were characterized, and they were demonstrated as a

promising adsorbent for Cd(II) and Pb(II) removal from aqueous solution. Solution pH, contact time, adsorbent dose, and initial metal concentration were investigated. The adsorption kinetics, isotherm models, thermodynamics, and reusability of metal ions onto magnetite were investigated.

EXPERIMENTAL

1. Chemicals and reagents

The chemicals used in this work were of analytical grade reagent. Ferric chloride was purchased from Qualikems fine chem. Pvt. Ltd., India. Ferrous sulphate and NaOH were obtained from the central drug house (P) Ltd., India. Cadmium chloride was purchased from LOBA Chemie, India.

2. Preparation of magnetite nanoparticles

Magnetite nanoparticles were synthesized by the co-precipitation method. By vigorous stirring at 60 °C, 1.9 g of FeSO₄·7H₂O and 3.9 g of FeCl₃·6H₂O were dissolved in distilled water (200 mL). This solution was treated by periodic probe sonication for 10 min. Then, to this solution, 10 M NaOH solution was added drop by drop under vigorous stirring at 60 °C until the pH was raised to 10-11 to precipitate the iron oxide. The mixture was additionally stirred on a magnetic stirrer at 60 °C for 2 h before being aged at room temperature for 24 h. After that, the formed magnetite nanoparticles were separated using a magnet and to achieve pH neutrality, they were washed several times with distilled water.

3. Characterization of magnetite nanoparticles

The prepared magnetite nanoparticles were X-ray diffracted using an X-ray diffractometer (Bruker D8 Advanced, Germany) with a Cu target (1.5406 Å) and a 2θ scanning range of 5° to 80°. The surface morphology of magnetite nanoparticles was provided using a scanning electron microscope (SEM Quanta FEG 250, the Netherlands). A high-resolution transmission electron microscope (model JEM-2100HRT, Japan) that operated at 200 kV was used to measure the particle size of magnetite nanoparticles. The FT-IR spectra of the produced magnetite nanoparticles were recorded using a Fourier-transform infrared (FTIR-6100 Jasco, Japan) spectrometer. The IR spectra were done using KBr pellets in the range of 4000–400 cm⁻¹ with a spectral resolution of 4 cm⁻¹ at room temperature.

4. Batch adsorption studies

The removal of Cd(II) or Pb(II) ion was performed in the batch technique from aqueous solutions by mixing 25 mL of each metal ion's solution with 0.05 g of the magnetite nanoparticles and shaking in a rotary shaker with a 180-rpm agitation speed at 25°C. To optimize the experimental conditions for the removal of each ion, various parameters such as pH in the range of 2 to 7, shaking time from 10 min to 3 h, the

dose of magnetite nanoparticles (0.01–0.2 g), initial Cd(II) or Pb(II) concentration from 5 to 400 mg L⁻¹, and temperature (25–55°C) were examined. After reaching equilibrium, a powerful magnet was used to separate the magnetite nanoparticles, and a 0.20 µm syringe filter was used to separate the supernatant. The residual concentration of the metal ions in the solution was determined using atomic absorption spectroscopy (240AAS, Agilent, USA). Using the following equation, the removal efficiency % of Cd(II) or Pb(II) was determined.

$$\text{Removal efficiency \%} = \frac{(C_i - C_e)}{C_i} \times 100 \quad (1)$$

where the initial and equilibrium metal ion concentrations in the solution (mg L⁻¹) are C_i and C_e, respectively. The adsorption capacity (q_e) of the prepared magnetite nanoparticles for Cd(II) or Pb(II) ion was estimated using equation 2:

$$q_e(\text{mg g}^{-1}) = \frac{(C_i - C_e) V}{m} \quad (2)$$

where V is the solution volume (L) and m is the magnetite dose (g) used.

5. Regeneration and reusability studies

The probability of regeneration and reuse of adsorbents has economic and environmental concern. For desorption experiments, Cd- and Pb-loaded magnetite nanoparticles were initially washed three times with distilled water to eliminate any loosely attached metal ions from their surface. The desorption process involved mixing 0.05g of Cd- and Pb-loaded magnetite nanoparticles with 10ml of 0.1 M HCl for 1h on a rotary shaker at an agitation speed of 180 rpm at 25°C. Desorption efficiency was determined by equation (3).

$$\text{Desorption efficiency \%} = \frac{\text{Concentration of released metal ion}}{\text{initial concentration of adsorbed metal ion}} \times 100 \quad (3)$$

The regenerated magnetite nanoparticles were tested for the reusability process by following the adsorption-desorption process for several cycles for both Cd(II) and Pb(II) removal.

RESULTS AND DISCUSSION

1. Characterization

1.1. XRD

Fig.1 depicts the XRD pattern of magnetite nanoparticles. The main peak at 35.65° is attributed to the crystalline plane with a miller index of (311). There are other noticeable diffraction peaks at 2θ of 30.27°, 43.33°, 53.77°, 57.32°, 62.95°, 67.26°, 71.43°, and 74.50°, which are indexed to (220), (400), (422), (511), (440), (442), (620) and (533) planes, respectively. All the diffraction peaks observed correspond to the magnetite nanoparticles standard pattern for JCPDS Card No.79-0417

(Geneti *et al.*, 2022). The estimated crystallite size of magnetite nanoparticles was 11.83 nm using Scherrer's formula (Cullity, 1956).

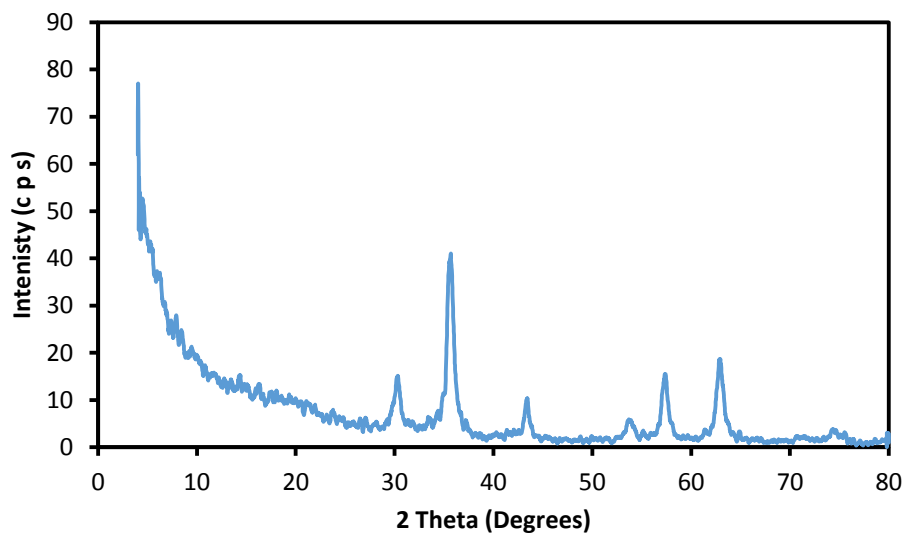


Fig. 1 XRD pattern of magnetite nanoparticles

1.2. TEM

TEM micrographs of the magnetite nanoparticles are shown in Fig. 2. It can be noted that magnetite exhibited irregular sphere-like particles. Additionally, the Fig. demonstrates that the particle size of magnetite nanoparticles ranged from ≈ 6 to 10 nm.

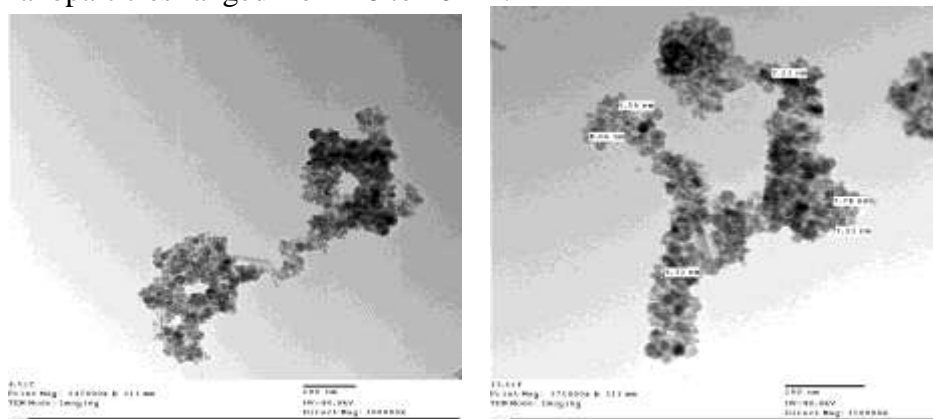


Fig. 2 TEM micrographs of magnetite nanoparticles

1.3. SEM/EDX

For describing the morphology, physical characteristics, and structure of the magnetite, SEM micrographs and EDX survey are crucial. The SEM images and EDX spectrum of the prepared magnetite

nanoparticles are shown in Fig. 3. The magnetite nanoparticles (Fig. 3 (a)) are agglomerated, stuck to each other, and have a spongy-like structure, as noticed from the micrograph. Fig. 3(b) reveals an EDX pattern with iron (85%) and oxygen (14%).

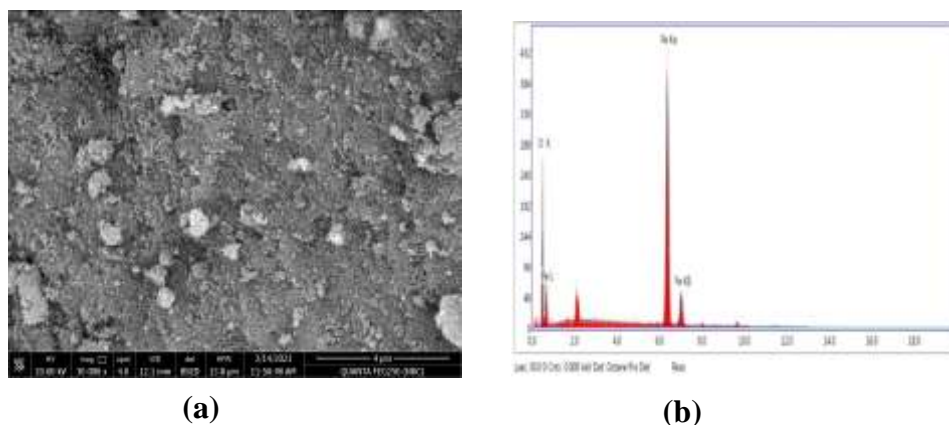


Fig. 3 SEM image (a) and EDX survey (b) of magnetite nanoparticles.

1.4. FT-IR

FT-IR spectrum of magnetite, as depicted in Fig. 4, presents strong absorption band at 544 cm^{-1} which is assigned to the Fe-O stretching vibration (**Geneti et al., 2022**). A significant peak at 834 cm^{-1} , corresponds to C-H bending (**Song et al., 2020 and Geneti et al., 2022**). The peak at 1061 cm^{-1} is ascribed to the C-O stretching vibration (**Singh et al., 2021**). The peak at 1632 cm^{-1} is assigned to the C = C stretching band (**Song et al., 2020 and Abatal et al., 2021**). The broad peak at around 3382 cm^{-1} indicated the O-H stretching vibration mode of the hydroxyl functional groups. The presence of the band at 2933 cm^{-1} may be attributed to the -CH_2 stretching vibration (**Geneti et al., 2022**).

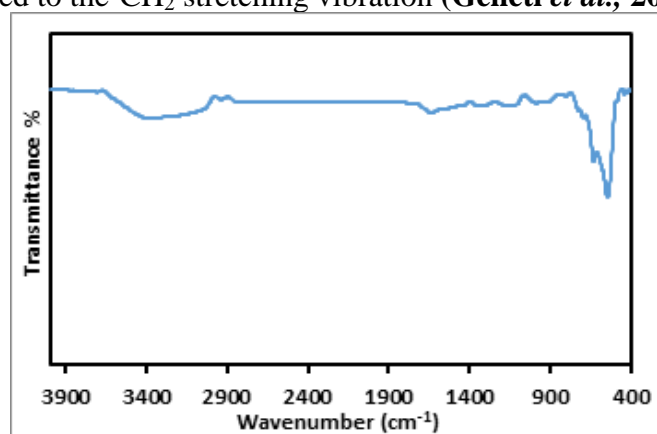


Fig. 4 FT-IR spectrum of magnetite nanoparticles.

2. Batch adsorption studies

2.1. Effect of initial pH

Experiments were performed to investigate the pH effect on Cd(II) and Pb(II) ions adsorption by magnetite in the pH range of 2-7. As seen in Fig. 5, Cd(II) and Pb(II) removal efficiencies increased with increasing the initial pH of the metal ion solution. It would be suggested that aqueous solutions with a higher pH value were favorable for the deprotonation of sorbent surfaces. Increased deprotonation may lead to an increase in negatively charged sites, which enhances the attractive forces between the surface of magnetite and the positively charged metal cations, increasing the removal of metal ions. Conversely, at low pH conditions, the magnetite surface is protonated, and becomes more positively charged. Thus, decreasing the adsorption of heavy metal ions as there is competition between protons and metal ions (Geneti *et al.*, 2022). As protons have a higher concentration and mobility, their adsorption would be preferred over metal ions. The adsorption process may be controlled by point zero charge pH (pH_{pzc}). The measured pH_{pzc} value for magnetite was found to be 5.5. It is clear that when the pH range is lower than pH_{pzc} , protonation of the magnetite nanoparticles surface occurs. Electrostatic repulsion reduced the adsorption capacity, preventing positive metal ions from reaching adsorption sites (Le *et al.*, 2019). The surface of the magnetite is negatively charged when the pH is greater than pH_{pzc} (Jain *et al.*, 2018), increasing the adsorption capacity as a result of electrostatic attraction between Cd(II) and Pb(II) ions and the surface of the magnetite.

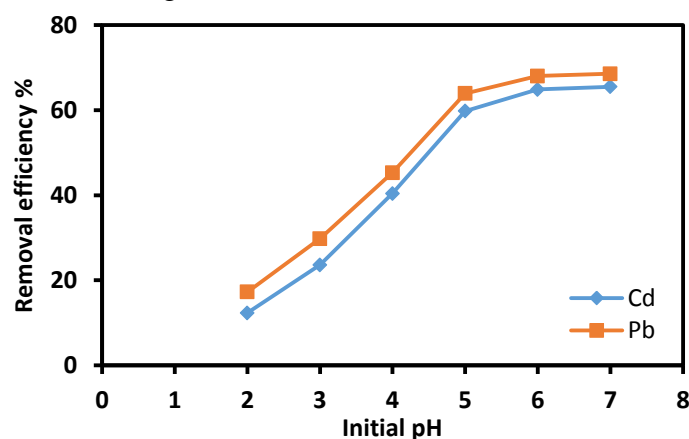


Fig. 5 Effect of initial pH on the adsorption of Cd(II) and Pb(II) using magnetite nanoparticles.

2.2. Effect of shaking time

The removal of Cd(II) and Pb(II) ions was carried out at varied time intervals (10 - 180 min), whereas the other process factors, such as temperature (25 °C), and initial metal concentration (50 mg L⁻¹) were kept constant. As shown in Fig. 6, the removal efficiency of Cd(II) and Pb(II) ions using magnetite nanoparticles increased with increasing the shaking time up to the equilibrium was attained. It is observed that the removal percentage was rapid for the first 10 min. The second stage can be done at a lower rate and there was a gradual increase till equilibrium, after which there was no important change in the Cd(II) and Pb(II) removal, and then the process reached saturated state. Generally, the rate of Cd(II) and Pb(II) ions removal was rapid initially, as available vacant surface sites in the magnetite were greater at the beginning of the adsorption process (Ghasemi *et al.*, 2018). Then slightly declines with the progress of time till they attain equilibrium (Geneti *et al.*, 2022). This is probably due to the exhausting of all vacant sites of magnetite. The experiments were run for 120 min to ensure complete adsorption of Cd(II) and Pb(II) ions from their solutions.

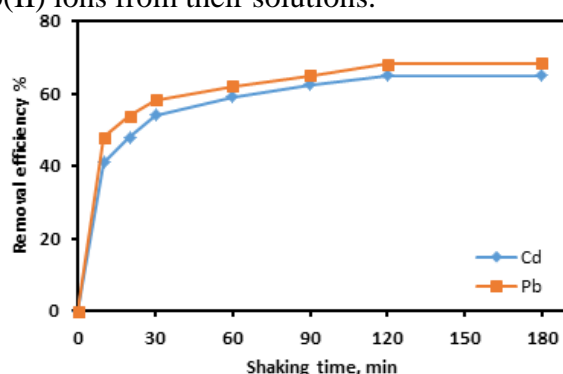


Fig. 6 Effect of shaking time on the removal of Cd(II) and Pb(II) using magnetite.

2.3. Effect of magnetite dose

The effect of magnetite nanoparticles dosage varying from 0.01 to 0.2 g for the removal of Cd(II) and Pb(II) ions keeping all other process variables constant is illustrated in Fig.7. The percentage removal of Cd(II) and Pb(II) ions was found to increase with an increase in magnetite dosage from 0.01 to 0.05 g. The removal of Cd(II) and Pb(II) ions increased with higher dose of the magnetite since the availability of more surface area and more adsorption sites to bind metal ions (Ghasemi *et al.*, 2018). The adsorption efficiency of metal ions was slightly affected by a further rise in the magnetite dose as the overcrowding of magnetite particles leads to interference of adsorption sites.

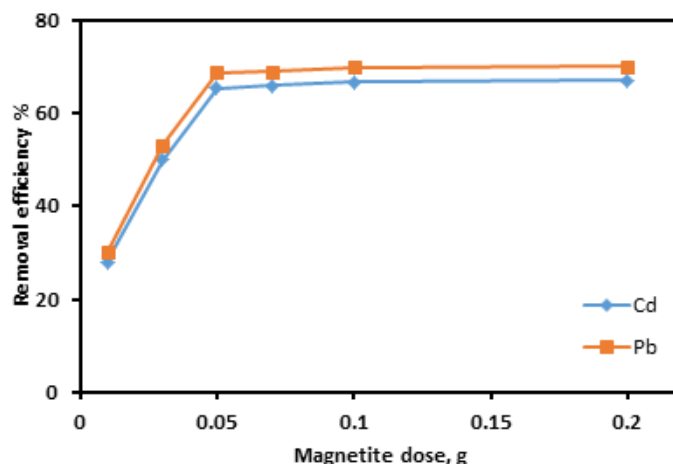


Fig. 7 Effect of magnetite dose on Cd(II) and Pb(II) adsorption.

2.4. Effect of metal ions' concentration

The effect of initial concentrations on the adsorption of Cd(II) and Pb(II) ions by magnetite nanoparticles was investigated at a range of 5 - 400 mg L⁻¹, while keeping all the other parameters constant and illustrated in Fig.8. As the initial Cd(II) and Pb(II) concentration rises, the mobility of metal ions increases and the diffusion of metal ions from the solution phase to the surface of magnetite increases, acting as a driving force for mass transfer between metal ions and adsorption sites (Le *et al.*, 2019). This causes collisions between metal ions and the surface of magnetite nanoparticles and increasing the adsorption capacity.

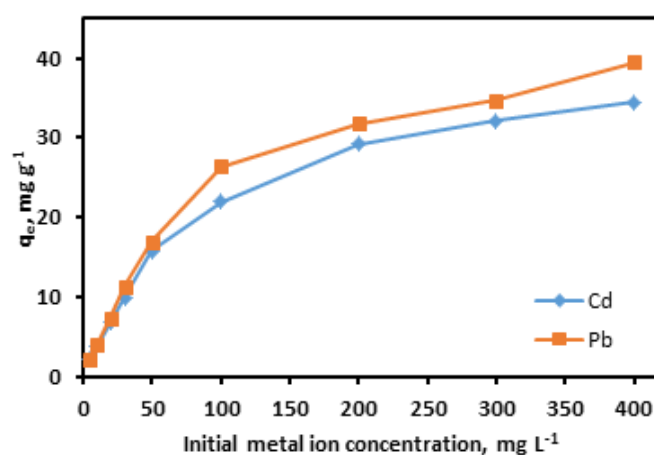


Fig. 8 Effect of initial Cd(II) and Pb(II) concentrations on their adsorption using magnetite.

3. Adsorption kinetics

In order to describe the adsorption rate and mechanism of Cd(II) and Pb(II) ions onto magnetite, the adsorption kinetic was used relating the adsorption process with time. To describe the adsorption kinetics, the Lagergren pseudo-first order, pseudo-second order, and intra-particle diffusion models were applied.

3.1. Lagergren pseudo-first-order model

The Lagergren's equation of pseudo first-order model supposes that one adsorbate is adsorbed onto one adsorption site on adsorbent surface. The linear form of pseudo first order model is given by Equation 4 :

$$\ln(q_e - q_t) = \ln q_e - k_1 t \quad (4)$$

where q_e and q_t (mg g^{-1}) are the amounts of Cd(II) and Pb(II) ions adsorbed at equilibrium and time t (min), respectively, and k_1 (min^{-1}) is the pseudo-first-order rate constant. The values of q_e and k_1 were estimated from the intercept and slope of the straight line, respectively, of plotting $\ln(q_e - q_t)$ versus t (Fig. 9 and Table 1). It's clearly shown that pseudo-first order kinetic model was not suitable to represent the adsorption kinetics of the adsorption of Cd(II) and Pb(II) ions onto magnetite because the estimated values of q_e are far from the found experimental q_e values.

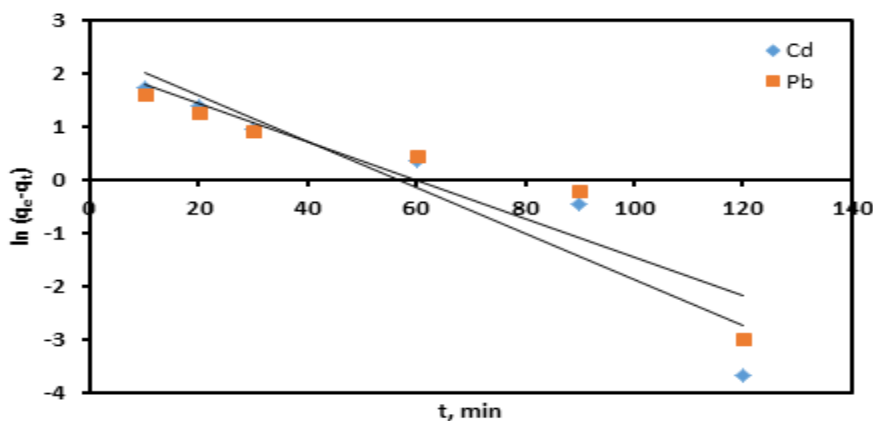


Fig. 9 Pseudo-first-order linear plots for the adsorption of Cd(II) and Pb(II) using magnetite nanoparticles.

3.2. Pseudo-second-order model

The linear form of pseudo-second order model is presented as:

$$\frac{t}{q_t} = \frac{1}{k_2 q_e^2} + \frac{t}{q_e} \quad (5)$$

where k_2 ($\text{g mg}^{-1} \text{min}^{-1}$) is the pseudo-2nd-order rate constant. The q_e and k_2 values are estimated from the slope and intercept of t/q_t versus time linear

plots (Fig. 10). Obviously, the relation between t/q_t and time for the Cd(II) and Pb(II) removal using magnetite is represented by a straight line. According to the results in Table 1, the pseudo-2nd-order model present the high correlation coefficients than pseudo-first-order for both Cd(II) and Pb(II) adsorption onto magnetite, and the experimental q_e values obtained are closer to those estimated for the pseudo-2nd--order kinetic model, confirming that the adsorption of Cd(II) and Pb(II) onto magnetite follows the pseudo-2nd--order kinetics (Qiu *et al.*, 2020 and Xiang *et al.*, 2021).

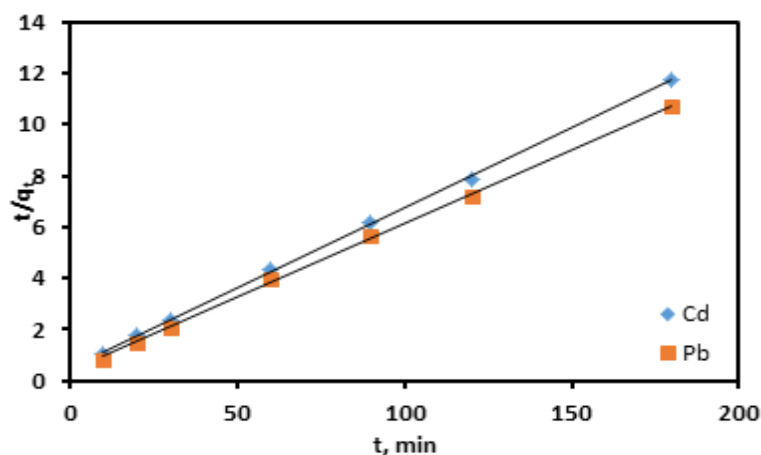


Fig. 10 Pseudo-second-order plots for the adsorption of Cd(II) and Pb(II) using magnetite nanoparticles.

3.3.3. Intra-particle diffusion model

The model of intra-particle diffusion can predict the mechanism of metal ions diffusion from the exterior surface into adsorbent pores. It plays an important role in determining the rate-controlling stage, and it was estimated using the Weber-Morris equation:

$$q_t = k_3 t^{0.5} + C \quad (6)$$

where k_3 is the rate constant of intra-particle diffusion ($\text{mg g}^{-1} \text{min}^{-0.5}$), and C is the intercept of the plot of q_t versus $t^{0.5}$ which is directly proportional to the thickness of the boundary layer. The values of k_3 and C are tabulated in Table 1, and the plots are shown in Fig. 11. A plot of q_t against $t^{0.5}$ will be linear and have a line that passes through the origin if intra-particle diffusion is the only controlling step. However, the line did not pass through the origin in the present study, indicating that intra-particle diffusion was not the only rate-determining step to control the adsorption of Cd(II) and Pb(II), but also effected by internal diffusion and membrane diffusion (Xiang *et al.*, 2021).

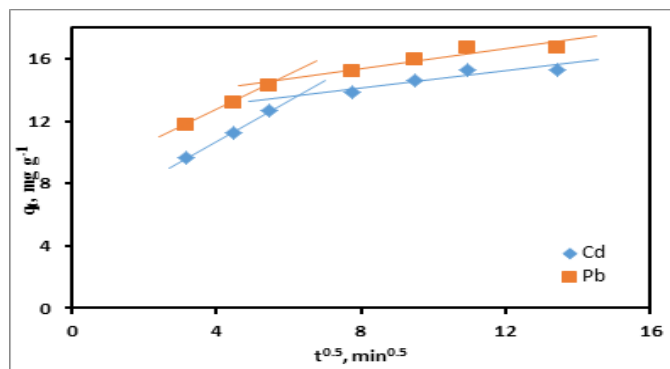


Fig. 11 Intra-particle diffusion plots for the adsorption of Cd(II) and Pb(II) ions using magnetite.

Table 1. Estimated parameters of the pseudo-first-order, pseudo-second-order and intra-particle diffusion models for Cd(II) and Pb(II) ions removal using magnetite.

Model	Parameter	Adsorbate	
		Cd(II)	Pb(II)
Pseudo-first-order	k_1 (min^{-1})	0.043	0.036
	$q_{e, \text{calc.}}$ (mg g^{-1})	11.36	8.70
	$q_{e, \text{exp.}}$ (mg g^{-1})	15.72	16.87
	R^2	0.8845	0.8751
Pseudo-second-order	k_2 ($\text{g mg}^{-1} \text{min}^{-1}$)	0.008	0.009
	$q_{e, \text{calc.}}$ (mg g^{-1})	16.01	17.35
	$q_{e, \text{exp.}}$ (mg g^{-1})	15.72	16.87
	R^2	0.9996	0.9994
Intra-particle diffusion	k_3 ($\text{mg g}^{-1} \text{min}^{-0.5}$)	1.317	1.083
	C	5.448	8.368
	R^2	0.9990	0.9998

4. Adsorption equilibrium studies

Adsorption isotherms express the mathematical relationship between the quantity of adsorbate and the equilibrium concentration of adsorbate remaining in the solution at a constant temperature. The equilibrium adsorption data has been analyzed using Langmuir, Freundlich, Dubinin–Radushkevich, and Temkin isotherms (Abatal *et al.*, 2021).

4.1. Langmuir isotherm

The Langmuir isotherm makes the assumption that an adsorbent has a finite number of identical, energetically equivalent binding sites. A single monolayer is created since each site can only adsorb one molecule. It is used to calculate an adsorbent's maximum adsorption capacity. The linearized Langmuir isotherm is expressed by:

$$\frac{C_e}{q_e} = \frac{1}{K_L q_{\text{max}}} + \frac{C_e}{q_{\text{max}}} \quad (7)$$

where q_{\max} (mg g^{-1}) is the maximum sorption capacity and K_L (L mg^{-1}) is the constant for the Langmuir model, which is correlated to the affinity of binding sites. By plotting the C_e/q_e versus C_e , the values of q_{\max} and K_L can be estimated. The experimental data for the adsorption of Cd(II) and Pb(II) using magnetite are listed in Table 2 and exactly fit the linear form of the Langmuir equation.

4.2. Freundlich isotherm

According to the Freundlich isotherm, sorbents have heterogeneous surfaces with various adsorption potential sites. Additionally, it presumes that stronger binding sites are occupied first, and that binding strength diminishes with increasing the degree of occupancy. It is given by:

$$\log q_e = \frac{1}{n} \log C_e + \log K_F \quad (8)$$

where K_F (mg g^{-1}) is the Freundlich constant, which represents adsorption capacity, and n (L mg^{-1}) is the adsorption intensity. The values of K_F and n (Table 2) can be estimated from the intercept and slope of the plot of $\log q_e$ versus $\log C_e$. The values of Freundlich constant "n", which measures the adsorption intensity of Cd(II) and Pb(II), were observed to be greater than 1, suggesting the adsorption process is physical (Afolabi *et al.*, 2021). The values of n between 1 and 10 suggest that the adsorption process is favorable (Nodeh *et al.*, 2019). As can be noticed from the Table 3, the correlation coefficient values (R^2) of the Langmuir model were higher in comparison with those of the Freundlich adsorption isotherm, thus indicating that the Langmuir model fitted the experimental adsorption data. This demonstrates that magnetite has a homogeneous distribution of active sites available for the adsorption of Cd(II) and Pb(II) onto its surface, and that monolayer adsorption is involved.

4.3. Dubinin–Radushkevich isotherm

The Dubinin–Radushkevich isotherm model (D-R) can be used to differentiate between physical and chemical adsorption processes and is expressed as:

$$\ln q_e = \ln K_{D-R} - \beta \varepsilon^2 \quad (9)$$

where the D-R constant is K_{D-R} (mg g^{-1}), and the Polanyi potential is ε ($\text{mol}^2 \text{J}^{-2}$), which is equal to:

$$\varepsilon = RT \ln \left(1 + \frac{1}{C_e} \right) \quad (10)$$

where T is the absolute temperature (K) and R is the universal gas constant ($\text{J K}^{-1} \text{mol}^{-1}$). The constant β is related to E (kJ mol^{-1}). The

energy E is defined as the free energy change required to transfer 1 mole of ions from the solution to the solid:

$$E = 1/\sqrt{2\beta} \quad (11)$$

The values of β and K_{D-R} (Table 2) can be obtained from the slope and intercept of the linear plot of $\ln q_e$ against ε^2 . The value of E offers information about the adsorption mechanism, if E value is less than 8 kJ mol^{-1} represent the physisorption process, and E value within the range of $8\text{--}16 \text{ kJ mol}^{-1}$ is assigned to the chemisorption process. Given that E values in this investigation were less than 8 kJ mol^{-1} , it was clear that the physisorption process was followed by the adsorption mechanism.

4.4. Temkin isotherm

The Temkin isotherm model describes the uniform distribution of binding energies. It implies that adsorbent-adsorbate interactions cause the adsorption energy to drop linearly with surface coverage. The Temkin isotherm is given by:

$$q_e = \frac{RT}{b_T} \ln A_T + \frac{RT}{b_T} \ln C_e \quad (12)$$

where b_T (kJ mol^{-1}) is the Temkin isotherm constant, which is related to adsorption heat, and A_T (L g^{-1}) is the equilibrium binding constant corresponding to the maximum binding energy. The values of A_T and b_T , which are given in Table 2, can be estimated from q_e versus $\ln C_e$ plots.

Table 2. The parameters of the Langmuir, Freundlich, Dubinin-Radushkevich (D-R), and Temkin isotherm models for the adsorption of Cd(II) and Pb(II) onto magnetite nanoparticles.

Isotherm model	Parameter	Adsorbate	
		Cd(II)	Pb(II)
Langmuir	K_L (L mg^{-1})	0.042	0.046
	q_{\max} (mg g^{-1})	36.20	40.10
	R^2	0.9964	0.9925
Freundlich	K_F	2.85	3.32
	$1/n$	0.475	0.468
	R^2	0.9542	0.9483
Dubinin-Radushkevich(D-R)	K_{D-R}	33.11	35.94
	$\beta \cdot 10^{-3}$	0.200	0.114
	E (kJ mol^{-1})	1.60	2.09
	R^2	0.9483	0.7845
Temkin	b_T (kJ mol^{-1})	0.413	0.383
	A_T (L g^{-1})	0.85	1.012
	R^2	0.9775	0.9755

5. Thermodynamics studies

The impact of temperature on the Cd(II) and Pb(II) ions adsorption using magnetite was evaluated at temperatures of 298, 308, 318, and 328

K by conducting experiments using 50 and 100 mg L⁻¹ of Cd(II) and Pb(II) initial concentrations, respectively. The thermodynamic parameters including Gibbs free energy change (ΔG°), enthalpy change (ΔH°), and entropy change (ΔS°) were obtained from the following equations:

$$\Delta G^\circ = \Delta H^\circ - T\Delta S^\circ \quad (13)$$

$$K_d = \frac{q_e}{C_e} \quad (14)$$

$$\ln K_d = \frac{\Delta S}{R} - \frac{\Delta H}{RT} \quad (15)$$

Equation (13) was used to calculate the values of ΔG° and the values of ΔH° and ΔS° values were obtained from the slope and intercept of the linear plot of $\ln K_d$ versus $1/T$ (Fig. 12). The calculated thermodynamics parameters are tabulated in Table 3. It can be noticed that ΔG° values diminished as the temperature increased, proposing that the high temperatures were preferred for the adsorption of Cd(II) onto magnetite nanoparticles, and an enhanced spontaneity with temperature. The positive values of ΔG° indicated that the adsorption of Pb(II) was unfavorable, and these positive values revealed that the adsorption of Pb(II) was non spontaneous in the studied range of temperature. The positive values of ΔS° demonstrated the enhanced randomness at the solid / liquid interface during the adsorption of both Cd(II) and Pb(II) onto magnetite (Xiang *et al.*, 2021). The positive values of ΔH° confirmed the adsorption process was endothermic, which was consistent with the increase in the percentage removal of metal ions with escalating temperature.

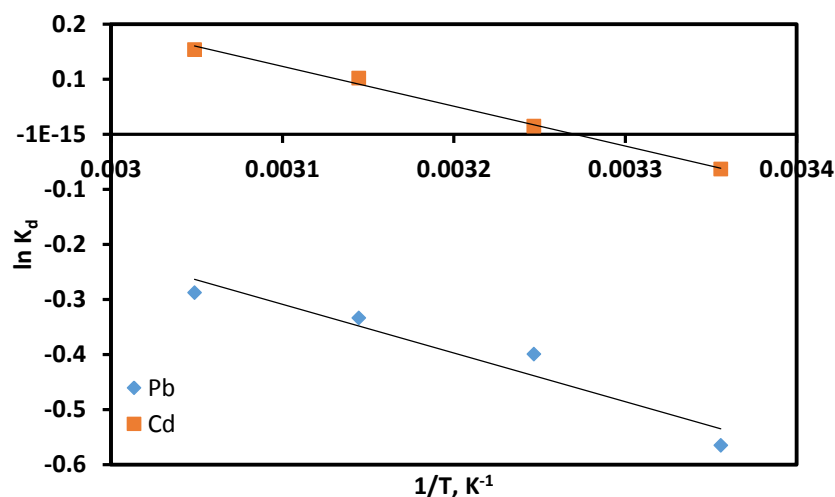


Fig. 12 Thermodynamic plots of Cd(II) and Pb(II) removal using magnetite nanoparticles.

Table 3. Thermodynamic parameters for adsorption of Cd(II) and Pb(II) onto magnetite.

Adsorbate	ΔH° (kJ mol ⁻¹)	ΔS° (J mol ⁻¹ K ⁻¹)	ΔG° (kJ mol ⁻¹)			
			298K	308K	318K	328K
Cd(II)	6.014	19.670	0.152	-0.045	-0.241	-0.438
Pb(II)	7.349	20.216	1.325	1.123	0.921	0.718

6. Regeneration and reusability studies

The reusability and possibility of regeneration of adsorbent are a significant index for evaluating the practical application potential of the prepared adsorbent. Magnetite reusability was studied by conducting several adsorption–desorption cycles. The desorption process was checked by using 10 mL of 0.1 M HCl with 0.05 g Pb and Cd-loaded magnetite nanoparticles for 1 h using an agitation speed of 180 rpm on a rotary shaker at 25°C. A strong magnet was used to separate the magnetite nanoparticles, the supernatant was collected to measure the desorbed Cd(II) and Pb(II) ions in the solution, then the desorption efficiencies were estimated. The desorption efficiency of Cd(II) and Pb(II) was found to be high for the first cycle. The desorption efficiency of Cd(II) was 92.56%, and of Pb(II) was 93.33% by magnetite. Fig. 13 shows that the removal efficiency was slightly reduced with the proceeding cycles up to five cycles.

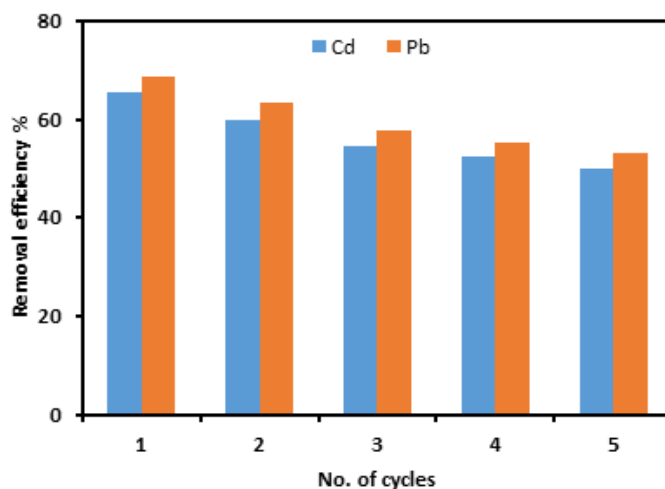


Fig. 13 Reusability of magnetite nanoparticles for the removal of Cd(II) and Pb(II).

CONCLUSION

Magnetite nanoparticles were prepared by using the commonly co-precipitation technique. The prepared adsorbent was characterized using different techniques and utilized for the Cd(II) and Pb(II) removal from aqueous solution. Magnetite nanoparticles have irregular like-spheres with particle sizes

in the range of $\approx 6\text{--}10$ nm. The Langmuir model provided a good fit to the experimental Cd(II) and Pb(II) removal equilibrium data. The pseudo second-order model was well correlated to the experimental data. Thermodynamically, the removal of Cd(II) and Pb(II) ions by the magnetite nanoparticles was endothermic and favorable. The prepared magnetite also offered excellent recyclability and stability up to five times of the adsorption-desorption cycles. In conclusion, the results showed that the prepared magnetite nanoparticles would be superior solution for wastewater treatment.

REFERENCES

- Abatal, M. ; M.T.Olguin ; I. Anastopoulos ; D.A. Giannakoudakis ; E.C.Lima ; J. Vargas and C. Aguilar (2021).** Comparison of heavy metals removal from aqueous solution by *Moringa oleifera* leaves and seeds. *Coatings*, 11(5). <https://doi.org/10.3390/coatings11050508>
- Afolabi, F.O. ; P.Musonge and B.F. Bakare (2021).** Bio-sorption of copper and lead ions in single and binary systems onto banana peels. *Cogent Engineering*, 8(1): 1886730.
- Akpomie, K.G. and J. Conradie (2020).** Advances in application of cotton-based adsorbents for heavy metals trapping, surface modifications and future perspectives. *Ecotoxicol. and Environ. Safety*, 201: 110825.
- Baby, R. ; B. Saifullah and M.Z. Hussein (2019).** Palm kernel shell as an effective adsorbent for the treatment of heavy metal contaminated water. *Scientific Reports*, 9(1): 1–11.
- Beni, A.A. and A. Esmaeili (2020).** Biosorption, an efficient method for removing heavy metals from industrial effluents: A review. *Environ. Technol. & Innovation*, 17: 100503.
- Cullity, B. D. (1956).** *Elements of X-ray Diffraction*. Addison-Wesley Publishing.
- Geneti, S.T. ; G.A.Mekonnen ; H.C. Murthy ; E.T.Mohammed ; C.R. Ravikumar ; B.A. Gonfa and F.K. Sabir (2022).** Biogenic synthesis of magnetite nanoparticles using leaf extract of *thymus schimperi* and their application for monocomponent removal of chromium and mercury ions from aqueous solution. *J. Nanomaterials*, 2022. <https://doi.org/10.1155/2022/5798824>
- Ghasemi, N. ; M.Ghasemi ; S. Moazeni ; P. Ghasemi ; N. S.Alharbi ; V.K.Gupta ; S.Agarwal ; I.V.Burakova and A.G. Tkachev (2018).** Zn (II) removal by amino-functionalized magnetic nanoparticles: Kinetics, isotherm, and thermodynamic aspects of adsorption. *J. Industrial and Eng. Chem.*, 62: 302–310.
- Jain, M. ; M.Yadav ; T.Kohout ; M.Lahtinen ; V.K.Garg and M.Sillanpää (2018).** Development of iron oxide/activated carbon nanoparticle composite for the removal of Cr(VI), Cu(II)

- and Cd(II) ions from aqueous solution. *Water Resources and Industry*, 20, 54–74. <https://doi.org/10.1016/j.wri.2018.10.001>
- Kumari, P. ; M. Alam and W.A. Siddiqi (2019).** Usage of nanoparticles as adsorbents for waste water treatment: An emerging trend. *Sustainable Materials and Technol.*, 22, e00128. <https://doi.org/10.1016/j.susmat.2019.e00128>
- Le, V.T. ; T.K.N.Tran ; D.L. Tran ; H.S.Le ; V.D.Doan ; Q.D. Bui and H.T.Nguyen (2019).** One-pot synthesis of a novel magnetic activated carbon/clay composite for removal of heavy metals from aqueous solution. *J. Dispersion Sci. and Technol.*, 40(12), 1761–1776.
- Liu, Q. ; Y.Li ; H.Chen ; J.Lu ; G.Yu ; M.Möslang and Y. Zhou (2020).** Superior adsorption capacity of functionalised straw adsorbent for dyes and heavy-metal ions. *J. Hazardous Materials*, 382: 121040.
- Nodeh, H.R. ; M.A. Kamboh ; W.A.W. Ibrahim ; B.H.Jume ; H. Sereshti and M.M. Sanagi (2019).** Equilibrium, kinetic and thermodynamic study of pesticides removal from water using novel glucamine-calix [4] arene functionalized magnetic graphene oxide. *Environ. Sci. Processes & Impacts*, 21(4): 714–726.
- Qiu, Y. ; Q. Zhang ; B.Gao ; M.Li ; Z. Fan ; W.Sang ; H.Hao and X. Wei (2020).** Removal mechanisms of Cr (VI) and Cr (III) by biochar supported nanosized zero-valent iron: Synergy of adsorption, reduction and transformation. *Environ. Pollution*, 265: 115018.
- Rajput, S. ; C.U.Pittman and D. Mohan (2016).** Magnetic magnetite (Fe₃O₄) nanoparticle synthesis and applications for lead (Pb²⁺) and chromium (Cr⁶⁺) removal from water. *J. Colloid and Interface Sci.*, 468: 334–346.
- Singh, A. ; S. Chaudhary and B.S. Dehiya (2021).** Fast removal of heavy metals from water and soil samples using magnetic Fe₃O₄ nanoparticles. *Environ. Sci. and Pollution Res.*, 28(4): 3942–3952.
- Song, X. ; Y. Zhang ; N. Cao ; D. Sun ; Z.Zhang ; Y.Wang ; Y.Wen ; Y.Yang and T. Lyu (2020).** Sustainable chromium (VI) removal from contaminated ground water using nano-magnetite-modified biochar via rapid microwave synthesis. *Molecules*, 26(1): 103.
- Umeh, C. ; J.N.Asegbeloyin ; K.G.Akpomie ; E.E.Oyeka and A.E.Ochonogor (2020).** Adsorption properties of tropical soils from Awka North Anambra Nigeria for lead and cadmium ions from aqueous media. *Chem. Afr.*, 3(1): 199–210.

- Vardhan, K.H. ; P.S.Kumar and R.C.Panda (2019).** A review on heavy metal pollution, toxicity and remedial measures: Current trends and future perspectives. J. Molecular Liquids, 290, 111197. <https://doi.org/10.1016/j.molliq.2019.111197>
- Xiang, L. ; C.G.Niu ; N.Tang ; X.X.Lv ; H.Guo ; Z.W.Li ; H.Y. Liu ; L.S.Lin ; Y.Y.Yang and C. Liang (2021).** Polypyrrole coated molybdenum disulfide composites as adsorbent for enhanced removal of Cr (VI) in aqueous solutions by adsorption combined with reduction. Chem. Eng. J., 408, 127281.
- Yu, X. and J. Jiang (2020).** Phosphate microbial mineralization consolidation of waste incineration fly ash and removal of lead ions. Ecotoxicol. and Environ. Safety, 191: 110224.
- Zhang, Z. ; T.Wang ; H.Zhang ; Y. Liu and B. Xing (2021).** Adsorption of Pb (II) and Cd (II) by magnetic activated carbon and its mechanism. Sci. Total Environ., 757: 143910.
- Zhou, Y. ; L.Luan ; B.Tang ; Y.Niu ; R. Qu ; Y. Liu and W. Xu (2020).** Fabrication of Schiff base decorated PAMAM dendrimer/magnetic Fe₃O₄ for selective removal of aqueous Hg (II). Chem. Eng. J., 398: 125651.

خصائص الامصاص لجزيئات الماجنتيت النانومترية لإزالة المعادن الثقيلة من

المحلول المائي

إيمان ربيع ذكي¹ - صابر محمود أحمد¹ - أمنية إبراهيم على² - مهجة شفيق عبدالله²

¹ معهد بحوث الأراضى والمياه والبيئة - مركز البحوث الزراعية - الجيزة - مصر

² قسم الكيمياء - كلية العلوم - جامعة حلوان - القاهرة - مصر

لقد تضمنت هذه الدراسة امكانية تطبيق جزيئات الماجنتيت النانومترية كمدمص قوي لإزالة أيونات الكاديوم (II) والرصاص (II) من المحاليل المائية باستخدام تقنية الدفعة. وقد تم توصيف جزيئات الماجنتيت النانومترية التي تم تصنيعها بواسطة تقنية الترسيب الكيميائي باستخدام قياسات XRD و SEM-EDX و TEM و FT-IR. وقد تم دراسة تأثير كل من الأس الهيدروجيني ، ومدة التفاعل ، وكتلة الماجنتيت ، وتركيز أيون الكاديوم والرصاص على كفاءة إزالة هذه الأيونات. وقد وجد ان بيانات الأدمصاص تتوافق مع معادلة لانجمير الايزوثرمية ومعادلة تفاعلات الرتبة الثانية. وقد تم اثبات ان عملية ادمصاص أيونات الكاديوم والرصاص بواسطة جزيئات الماجنتيت النانومترية من خلال المعاملات الديناميكية الحرارية عملية ماصة للحرارة. وقد ثبت انه من الممكن اعادة استخدام جزيئات الماجنتيت النانومترية باستخدام حمض الهيدروكلوريك بكفاءة تصل الى خمس مرات. ولذلك فانه من الممكن استخدام جزيئات الماجنتيت النانومترية كمواد ممدصة بديلة وصديقة للبيئة لازالة أيونات الكاديوم والرصاص.